

# Pulling a DNA molecule through a nanopore embedded in a charged membrane: tension propagation against electrostatics

Jalal Sarabadani,<sup>1,\*</sup> Sahin Buyukdagli,<sup>2,†</sup> and Tapio Ala-Nissila<sup>3,4,‡</sup>

<sup>1</sup>*School of Nano Science, Institute for Research in Fundamental Sciences (IPM), 19395-5531, Tehran, Iran*

<sup>2</sup>*Department of Physics, Bilkent University, Ankara 06800, Turkey*

<sup>3</sup>*Department of Applied Physics and QTF Center of Excellence,*

*Aalto University, P.O. Box 11000, FI-00076 Aalto, Espoo, Finland*

<sup>4</sup>*Interdisciplinary Centre for Mathematical Modelling and Department of Mathematical Sciences, Loughborough University, Loughborough, Leicestershire LE11 3TU, United Kingdom*

We consider the influence of electrostatic forces on driven translocation dynamics of a flexible polyelectrolyte being pulled through a nanopore by an external force on the head monomer. To this end, we augment the iso-flux tension propagation (IFTP) theory with electrostatics for an anionic biopolymer pulled through a nanopore embedded in a cationic membrane. We show that for the realistic case of an anionic polyelectrolyte such as a single-stranded DNA, the translocation dynamics at low salt where screening is weak and at finite positive membrane charge, is governed by the attractive electrostatic interactions between the polymer coil on the *cis* side and the charged membrane. These interactions result in a non-monotonic polymer length and membrane charge dependence of the exponent  $\alpha$  characterizing the translocation time  $\tau \propto N_0^\alpha$  of the polymer with length  $N_0$ . Due to the same electrostatic polymer-membrane coupling, in the regime of long polymers  $N_0 \gtrsim 500$ , the translocation exponent exceeds its upper limit  $\alpha = 2$  previously observed for the same system without electrostatic interactions.

## I. INTRODUCTION

Polymer translocation through a nanopore has been subject of numerous studies during the last two decades [1–5] following the seminal works by Bezrukov *et al.* in 1994 [6] and later by Kasianowicz *et al.* in 1996 [7]. It has many technological applications in rapid DNA sequencing [7–11], drug delivery [12] and gene therapy. Motivated by these, many experimental [13–18] as well as theoretical [19–44] works have been published in this research field during the last twenty years or so.

From a theoretical point of view, many studies have been devoted to elucidate the physics of uncharged polymer translocation through a nanopore embedded in an uncharged membrane when driven by an external force. In 2007 Sakaue came up with the idea of tension propagation (TP) in the context of driven polymer translocation [24]. A quantitative theory was developed starting in 2012 when Ikonen *et al.* showed that driven translocation processes can be described by using the TP formalism in the context of Brownian dynamics [27, 30]. Using the TP formalism together with the iso-flux assumption (IFTP) [25] several different scenarios such as pore-driven translocation of a flexible and semi-flexible chain through a nanopore [27, 30, 32], pore-driven flexible polymer translocation under an alternating driving force through a flickering pore [31], and end-pulled polymer translocation through a nanopore [33], have been investigated.

In the TP formalism for driven translocation, a tension front propagates along the backbone of the subchain on the *cis* side. This is called TP stage, where the tension has not reached the chain end yet. Therefore, the subchain on the *cis* side is divided into two parts, namely a mobile part wherein the monomers move with net non-zero velocities towards the pore, and an equilibrium part where the monomers' average velocities in a narrow window of time are close to zero due to the random thermal fluctuations caused by the solvent. Finally, the tension reaches the chain end and the post propagation (PP) stage starts. This lasts until the whole mobile subchain on the *cis* side is sucked into the pore.

In the pore-driven case, as the relative dielectric constant of the solvent is typically high ( $\approx 80$ ) with respect to that of the membrane ( $\approx 2 - 4$ ), it is a good approximation to assume that an external force acts on the monomers located inside the nanopore only. However, in many cases of biological and experimental interest it is relevant to consider polyelectrolytes that are charged, such as DNA. This requires taking into account both the presence of counterions in the solution and the dielectric properties of the membrane through which the polyelectrolyte is translocating. Recently there has been an intense effort to model polyelectrolyte translocation including the details of the pore electrohydrodynamics and/or electrostatic polymer-membrane interactions, however, with the price of neglecting conformational polymer fluctuations [5, 39–43]. This simplified modeling has allowed to characterize the electrohydrodynamic mechanism of experimentally observed DNA mobility reversal by charge inversion [45] and pressure-voltage traps [46], and also enabled to identify strategies for faster polymer capture and slower translocation required for accurate biosequencing.

\*Electronic address: jalal@ipm.ir

†Electronic address: buyukdagli@fen.bilkent.edu.tr

‡Electronic address: Tapio.Ala-Nissila@aalto.fi

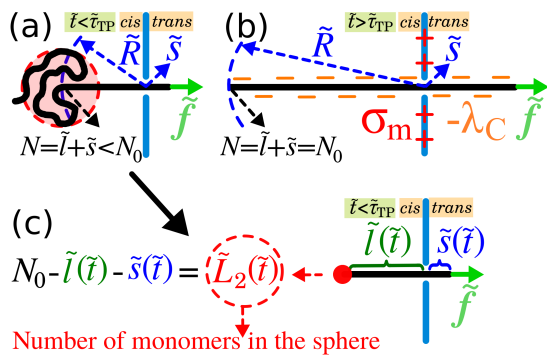


FIG. 1: (a) A schematic of end-pulled polymer translocation through a nanopore in the tension propagation stage.  $\tilde{R}$  and  $\tilde{s}$  are the distances of the tension front from the pore entrance and translocation coordinate, respectively.  $N = \tilde{l} + \tilde{s} < N_0$  is the number of beads that have already influenced by the tension,  $\tilde{l}$  is the number of beads in the mobile subchain on the *cis* side, and  $N_0$  in the polymer contour length. The external driving force  $\tilde{f}$  acts on the head monomer of the polymer only. (b) The same as panel (a) but in the post propagation stage, where the tension has already reached the chain end and  $\tilde{l} + \tilde{s} = N_0$ .  $\sigma_m > 0$  and  $-\lambda_C < 0$  are positive surface and negative linear charge densities distributed on the membrane and on the polymer, respectively (not shown in panels a and c). (c) The electric charge inside the polymer coil (sphere) in panel (a) (highlighted by the red color) is approximated by a point charge (red dot) including  $\tilde{L}_2(\tilde{t}) = N_0 - \tilde{l}(\tilde{t}) - \tilde{s}(\tilde{t})$  monomers. See text for further details and definition of dimensionless variables denoted by a tilde.

In this letter, we undertake the ambitious task to develop a unified theory of polymer translocation accounting for both tension propagation in a flexible chain and the electrostatic interactions between an anionic polymer and a cationic membrane when pulled through the membrane by an external force on the head monomer. Within this electrostatically augmented IFTP formalism, we characterize the competition between the electrostatic forces on the polyelectrolyte and the additional effect of the tension propagation mechanism.

## II. MODEL

It is a difficult challenge to include both electrostatic interactions and dynamics of tension propagation in a flexible chain on the same footing. During translocation a flexible polymer samples complicated time-dependent configurations leading into highly varying electrostatic interactions. To make this tractable, we will consider here a simplified model where we take into account the average interaction at any given moment during end-pulled translocation. Our theoretical model of an anionic polymer translocating through a cationic membrane nanopore is depicted in Fig. 1. The polymer is composed of  $N_0$  monomers and the external driving force only acts

on the head monomer. Within the framework of the IFTP theory, the charge-free version of this model has been studied in detail in Ref. [33]. As it has been shown in Refs. [4, 30, 33], in the pore-driven case, three different regimes exist for the *cis* side: the trumpet (TR), stem-flower (SF) and strongly stretching (SS) regimes, corresponding to weak, moderate and strong external driving force, respectively (in the limit of very weak force, Sakaue has presented additional scenarios [34]). For the end-pulled case, as both the *cis* and *trans* side subchains contribute to the translocation dynamics, complicated scenarios of multiple regimes are involved in the theory [33]. Here, as the main goal is to illustrate how the electrostatic interactions affects the average polymer translocation dynamics, for both the *cis* and *trans* side subchains we consider only the SS regime characterized by an external driving force satisfying the inequality  $\tilde{f} \gtrsim N_0$  (see below for the definitions of dimensionless variables denoted by tilde).

Here we also assume that the linear self-avoiding flexible polymer chain is negatively charged such as a DNA molecule, with a linear charge density of  $-\lambda_C < 0$ . Moreover, we assume that the translocated membrane carries a positive charge with surface charge density  $\sigma_m > 0$ . The positive membrane charge is a consequence of a high degree of protonation occurring in low pH conditions (or high bulk  $H^+$  concentration) for amphoteric substrates such as silicon-based membranes [42].

In the SS regime during the TP stage, the fully straightened *cis* and *trans* portions of the mobile sub-chain have lengths  $\tilde{l}$  and  $\tilde{s}$ , respectively. Then, the immobile part on the *cis* side is coiled as highlighted in Fig. 1(a) in light red color. The coil is assumed to be approximately spherical in shape in which case it can be modeled as a negative point charge (red dot in Fig. 1(c)). As depicted in Fig. 1(c), the number of monomers inside the sphere is  $\tilde{L}_2(\tilde{t}) = N_0 - \tilde{l}(\tilde{t}) - \tilde{s}(\tilde{t})$ . The boundary between the mobile polymer portion and the inert coil on the *cis* side is the position of the tension front, located at distance  $\tilde{R}$  from the pore entrance. The SS regime is characterized by the equality  $\tilde{R} = \tilde{l}$ . As time passes and tension propagates along the backbone of the chain, the number of monomers inside the sphere decreases, and therefore its size shrinks. The PP stage ends when the tension reaches the chain end and the sphere disappears. In the subsequent TP stage, the whole chain in both *cis* and *trans* sides is mobile and fully straightened.

To mathematically formulate the model presented above, we will first express the relevant physical parameters in dimensionless units, denoted by a tilde and defined as  $\tilde{Z} \equiv Z/Z_u$  [4, 27, 30, 31, 33]. The length, time, friction, force, velocity and monomer flux are written in units of  $s_u \equiv \sigma$ ,  $t_u \equiv \eta\sigma^2/(k_B T)$ ,  $\Gamma_u \equiv \eta$ ,  $f_u \equiv k_B T/\sigma$ , and  $\varphi_u \equiv k_B T/(\eta\sigma^2)$ , respectively, where  $\sigma$  is the segment length (or the size of each bead),  $k_B$  the Boltzmann constant, and  $T$  and  $\eta$  the solvent temperature and friction per monomer, respectively. The linear polymer charge density is expressed in units of  $\lambda_{C,u} \equiv e/\sigma$ , with the elec-

tron charge  $e = 1.6 \times 10^{-19}\text{C}$  and the Kuhn length of a single DNA strand  $\sigma = 1.5$  nm. Lennard-Jones units are used for quantities without the tilde, such as the friction, time and force.

In the SS regime, the spatial fluctuations of the straightened subchains on the *cis* and *trans* sides are negligible. Thus, it is sufficient to use the deterministic version of the IFTP theory without the entropic force term [27, 28, 30–32]. Within our electrostatically augmented IFTP formalism, the equation of motion for the translocation coordinate  $\tilde{s}$  corresponding to the number of beads on the *trans* side reads

$$\tilde{\Gamma}(\tilde{t}) \frac{d\tilde{s}}{d\tilde{t}} = \tilde{f} + \tilde{f}_{\text{pm}}^{\text{a}} \equiv \tilde{f}_{\text{tot}}, \quad (1)$$

where  $\tilde{\Gamma}(\tilde{t})$  stands for the effective friction coefficient,  $\tilde{f}$  is the external driving force acting on the head monomer of the polymer and oriented from the *cis* to *trans* side,  $\tilde{f}_{\text{pm}}^{\text{a}}$  is the electrostatic force due to the interaction between the opposite charges of the polymer and the membrane, the index  $\text{a} = \{\text{TP}, \text{PP}\}$  indicates the translocation stage, and  $\tilde{f}_{\text{tot}}$  is the total force. The effective friction that contains the essential physics of the tension propagation theory is defined as  $\tilde{\Gamma}(\tilde{t}) = \tilde{\eta}_{\text{p}} + \tilde{\eta}_{\text{cis}}(\tilde{t}) + \tilde{\eta}_{\text{TS}}(\tilde{t})$ , where  $\tilde{\eta}_{\text{p}}$  stands for the pore friction. Then,  $\tilde{\eta}_{\text{cis}}(\tilde{t})$  and  $\tilde{\eta}_{\text{TS}}(\tilde{t})$  are the solvent friction coefficients associated with the mobile subchain on the *cis* and *trans* sides, respectively. In the SS regime where the *cis* and *trans* portions of the polymer are straight lines, the hydrodynamic friction coefficient on each side is proportional to the length of the corresponding polymer portion, i.e.  $\tilde{\eta}_{\text{cis}}(\tilde{t}) = \tilde{l}(\tilde{t}) = \tilde{R}(\tilde{t})$  and  $\tilde{\eta}_{\text{TS}}(\tilde{t}) = \tilde{s}(\tilde{t})$ . Therefore, the total effective friction is given by

$$\tilde{\Gamma}(\tilde{t}) = \tilde{R}(\tilde{t}) + \tilde{s}(\tilde{t}) + \tilde{\eta}_{\text{p}}. \quad (2)$$

In Eq. (1), the electrostatic force on the polyelectrolyte reads  $\tilde{f}_{\text{pm}}^{\text{a}} = -\partial\tilde{\Omega}_{\text{pm}}^{\text{a}}/\partial\tilde{s}$ , where  $\tilde{\Omega}_{\text{pm}}^{\text{a}}$  stands for the electrostatic polymer-membrane interaction energy. The latter is given in the TP and PP stages by  $\tilde{\Omega}_{\text{pm}}^{\text{TP}} = -2\tilde{\lambda}_{\text{C}}[2 - e^{-\tilde{\kappa}_{\text{b}}\tilde{l}(\tilde{t})} - e^{-\tilde{\kappa}_{\text{b}}\tilde{s}(\tilde{t})}]/(\tilde{\mu}\tilde{\kappa}_{\text{b}}^2) - \tilde{\lambda}_{\text{C}}L_2(\tilde{t})\tilde{\phi}_{\text{m}}[\tilde{l}(\tilde{t})]$  and  $\tilde{\Omega}_{\text{pm}}^{\text{PP}} = -2\tilde{\lambda}_{\text{C}}[2 - e^{-\tilde{\kappa}_{\text{b}}\tilde{l}(\tilde{t})} - e^{-\tilde{\kappa}_{\text{b}}\tilde{s}(\tilde{t})}]/(\tilde{\mu}\tilde{\kappa}_{\text{b}}^2)$  [43], respectively, where we used the Debye-Hückel screening parameter  $\kappa_{\text{b}} = \sqrt{8\pi\ell_{\text{B}}\rho_{\text{b}}}$  and the Gouy-Chapman length  $\mu = e/(2\pi\ell_{\text{B}}|\sigma_{\text{m}}|)$ , with the Bjerrum length  $\ell_{\text{B}} = e^2/(4\pi\epsilon_0\epsilon_{\text{w}}k_{\text{B}}T) \approx 7$  Å at solvent temperature  $T = 300$  K and permittivity  $\epsilon_{\text{w}} = 80$ , and the salt concentration  $\rho_{\text{b}}$ . Moreover,  $L_2(\tilde{t}) = N_0 - \tilde{l}(\tilde{t}) - \tilde{s}(\tilde{t})$  is the number of beads in the coiled sphere, and  $\tilde{\phi}_{\text{m}}[\tilde{l}(\tilde{t})] = 2e^{-\tilde{\kappa}_{\text{b}}\tilde{l}(\tilde{t})}/(\tilde{\mu}\tilde{\kappa}_{\text{b}})$  stands for the membrane potential. The contribution from the electrostatic force  $\tilde{f}_{\text{pm}}^{\text{a}}$  to the force-balance equation

(1) is then obtained as

$$\tilde{f}_{\text{pm}}^{\text{TP}} = \frac{2\tilde{\lambda}_{\text{C}}}{\tilde{\mu}\tilde{\kappa}_{\text{b}}} \left[ + e^{-\tilde{\kappa}_{\text{b}}\tilde{s}(\tilde{t})} - e^{-\tilde{\kappa}_{\text{b}}\tilde{l}(\tilde{t})} - \tilde{\kappa}_{\text{b}}L_2(\tilde{t})e^{-\tilde{\kappa}_{\text{b}}\tilde{l}(\tilde{t})} \frac{\partial\tilde{l}(\tilde{t})}{\partial\tilde{s}(\tilde{t})} \right]; \quad (3)$$

$$\tilde{f}_{\text{pm}}^{\text{PP}} = \frac{2\tilde{\lambda}_{\text{C}}}{\tilde{\mu}\tilde{\kappa}_{\text{b}}} \left[ \frac{\partial\tilde{l}(\tilde{t})}{\partial\tilde{s}(\tilde{t})} e^{-\tilde{\kappa}_{\text{b}}\tilde{l}(\tilde{t})} + e^{-\tilde{\kappa}_{\text{b}}\tilde{s}(\tilde{t})} \right]. \quad (4)$$

At this point, we note that a key novelty of our model is the non-trivial time-dependence of the derivative term  $\partial\tilde{l}(\tilde{t})/\partial\tilde{s}(\tilde{t})$  in Eqs. (3) and (4). The resulting function originating from the presence of the charged sphere accounts for the coupling between the electrostatic polymer-membrane interactions and the tension propagation along the polymer chain. Thus, through this coupling, the present formalism goes beyond the purely electrostatic model of Ref. [43].

As mentioned above, in the SS regime the mobile subchain is fully straightened, i.e.  $\tilde{l} = \tilde{R}$ . In order to evaluate the derivative  $\partial\tilde{l}(\tilde{t})/\partial\tilde{s}(\tilde{t})$  in Eqs. (3) and (4), it should be noted that  $\tilde{R}$  is equivalent to the end-to-end distance of the flexible self-avoiding chain, i.e.  $\tilde{R} = A_{\nu}N^{\nu}$ , where  $N = \tilde{l} + \tilde{s}$  is the number of all monomers that have been already influenced by the tension force (see Fig. 1(a)), with the proportionality coefficient  $A_{\nu} = 1.15$  (for a coarse-grained bead-spring model as here), and the 3D Flory exponent  $\nu = 0.588$ . Then, in the PP stage, the mass conservation implies  $N_0 = \tilde{l} + \tilde{s}$  (see Fig. 1(b)). Therefore, the change in  $\tilde{l} = \tilde{R}$  with respect to the translocation coordinate  $\tilde{s}$  reads  $\partial\tilde{R}/\partial\tilde{s} = \nu A_{\nu}^{1/\nu} \tilde{R}^{(\nu-1)/\nu} / [1 - \nu A_{\nu}^{1/\nu} \tilde{R}^{(\nu-1)/\nu}]$  and  $\partial\tilde{R}/\partial\tilde{s} = -1$  in the TP and PP stages, respectively. Inserting the above equalities for  $\partial\tilde{R}/\partial\tilde{s}$  together with the mass conservation in the TP and PP stages into Eqs. (3) and (4), the IFTP Eqs. (1) and (2) in the TP and PP stages can be expressed solely in terms of the coordinate  $\tilde{l}$ . The explicit form of the corresponding equations and asymptotic analytical predictions will be presented in a future work. Finally, the function  $\tilde{l}(\tilde{t})$  obtained from the numerical solution of Eqs. (1) and (2) should be used in the scaling law  $\tilde{l} = A_{\nu}(\tilde{l} + \tilde{s})^{\nu}$  and  $N_0 = \tilde{l} + \tilde{s}$  to obtain the time dependence of the translocation coordinate  $\tilde{s}(\tilde{t})$  in the TP and PP stages, respectively.

### III. RESULTS

In order to describe the dynamics of the translocation process at the monomer level, we first examine the waiting time (WT), which is the time that each bead spends in the pore during translocation. We then illustrate the global dynamics of the translocation process by focusing on the translocation exponent  $\alpha$ , which is defined as  $\tau \propto N_0^{\alpha}$ , where  $\tau$  is the average translocation time and  $N_0$  the contour length of the polymer.

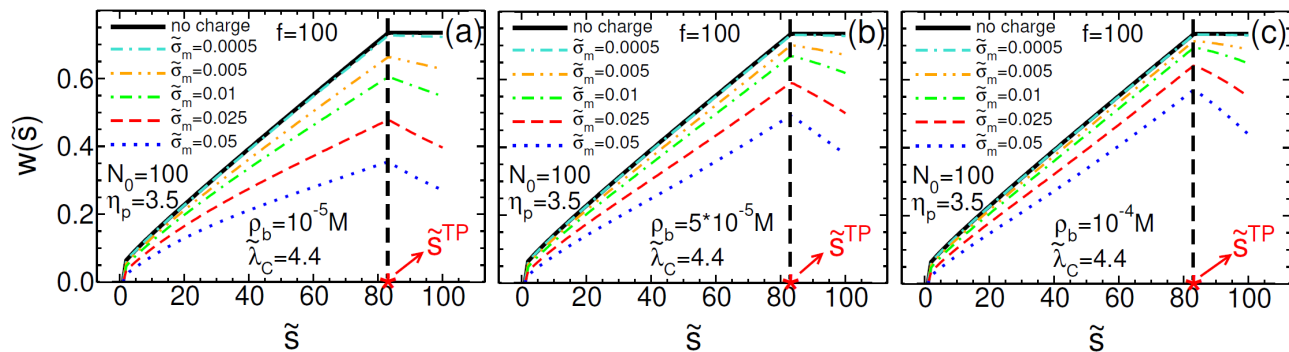


FIG. 2: (a) The waiting time  $w(\tilde{s})$  as a function of the translocation coordinate  $\tilde{s}$  for various values of the positive membrane charge density  $\tilde{\sigma}_m$  with constant chain length  $N_0 = 100$ , pore friction  $\eta_p = 3.5$ , external driving force  $f = 100$ , salt concentration  $\rho_b = 10^{-5}$  M, and the negative polymer line charge density  $\lambda_C = 1/3.4 e/\text{\AA}$  (or  $\tilde{\lambda}_C = 4.4$ ) of a single-stranded DNA molecule [43]. Panels (b) and (c) are the same as (a) but for different values of the salt concentrations  $\rho_b = 5 \times 10^{-5}$  M, and  $10^{-4}$  M, respectively. In all panels the translocation coordinate at the TP time is denoted by  $\tilde{s}^{\text{TP}}$  in red color.

### A. Waiting time

To characterize the effect of polymer-membrane interactions on the translocation dynamics, the WT is plotted in Figs. 2(a)-(c) as a function of the translocation coordinate  $\tilde{s}$ . The plots also display in red the translocation coordinate  $\tilde{s}^{\text{TP}}$  at the TP time corresponding to the time that takes for the tension front to reach the chain end. The WT curves were plotted for three different bulk salt concentrations ranging from  $\rho_b = 10^{-5}$  M to  $10^{-4}$  M, and various values of the positive membrane charge density  $\sigma_m$  increasing from top to bottom (see the legends). We consider here the dilute salt regime where the electrostatic interactions are weakly screened and expected to play an important role. It should be noted that this low salt concentration regime has been previously reached by translocation experiments [45]. The line charge density of the polymer is set to the value  $\lambda_C = 1/3.4 e/\text{\AA}$  corresponding to a single-stranded DNA molecule. The remaining model parameters are given in the caption of Fig. 2. We finally emphasize that because the electrostatic force in Eqs. (3) and (4) involve simply the product of the membrane and polymer charge densities, the results of our manuscript can be extrapolated to polyelectrolytes of different charge strengths by rescaling the membrane charge density value.

Figures 2(a)-(c) show that at constant salt concentration, the increment of the membrane charge density decreases the WT, i.e.  $\sigma_m \uparrow w(s) \downarrow$ . This trend originates from the amplification of the electrostatic polymer-membrane attraction with the membrane charge, which results in the acceleration of the translocation dynamics. Consequently, the TP time corresponding to the integral of the WT curve from zero to  $\tilde{s}^{\text{TP}}$  decreases with the increase of the membrane charge strength. One can also see from the figure that at constant membrane charge density, the increment of the bulk salt rapidly screens out the electrostatic polymer-membrane attrac-

tion. Figures 2(a)-(c) indicate that this leads to an increase of the WT and results in slower translocation rate, i.e.  $\rho_b \uparrow w(s) \uparrow$ . One finally notes that interestingly, the translocation coordinate  $\tilde{s}^{\text{TP}}$  at the TP time remains unaffected by the value of the surface charge density and the salt concentration. This shows that the electrostatics do not directly affect where the initiation of the post-propagation occurs in the chain.

### B. Translocation time exponent

Accurate polymer sequencing by translocation requires the extension of the ionic current blockade caused by the translocating polymer and thus the prolongation of the translocation event. Therefore, it is essential to characterize the effect of the experimentally tunable electrostatic model parameters on the total translocation time  $\tau$  for the entire polymer chain to translate from the *cis* to the *trans* side.

As seen in Figs. 2(a)-(c), at constant salt concentration, the translocation time corresponding to the integral of the WT time curve over the translocation coordinate  $s$  drops with the increase of the membrane charge, i.e.  $\sigma_m \uparrow \tau \downarrow$ . Moreover, the comparison of the panels (a)-(c) at constant surface charge indicates that due to electrostatic screening, the addition of bulk salt increases the translocation time and slows down the translocation dynamics, i.e.  $\rho_b \uparrow \tau \uparrow$ .

An exact scaling form for the translocation time in the SS regime for an end-pulled polymer chain has been derived in Ref. [33]. In the asymptotic limit of very long chains  $\alpha = 2$ , with large correction-to-scaling terms arising from the pore friction and the *trans* side friction of the chain. In order to understand the effect of electrostatic polymer-membrane interactions on the dependence of the translocation time on the contour length, we illustrate in Fig. 3 the effective translocation time exponent

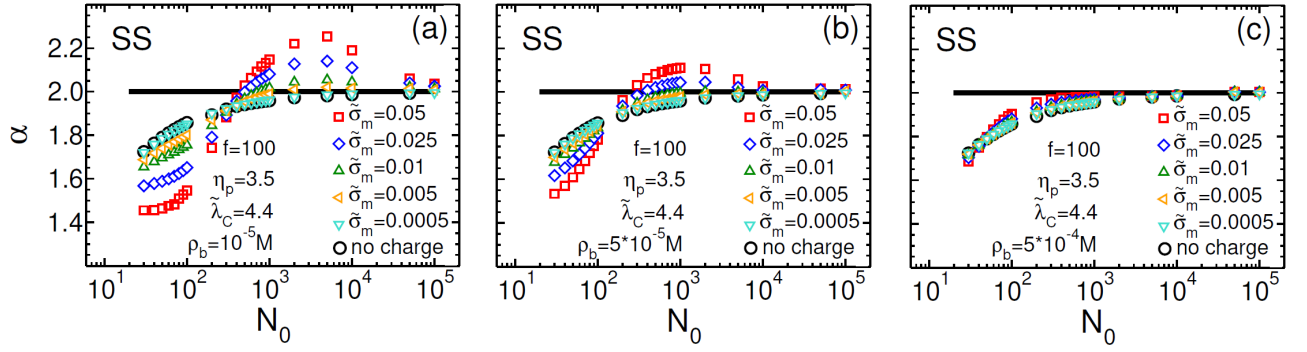


FIG. 3: (a) Translocation time exponent  $\alpha$  as a function of the polymer contour length for various values of the membrane charge density. The black horizontal line is the asymptotic limit  $\alpha = 2$  for uncharged chains. The model parameters given in the legend are the same as in Fig. 1.

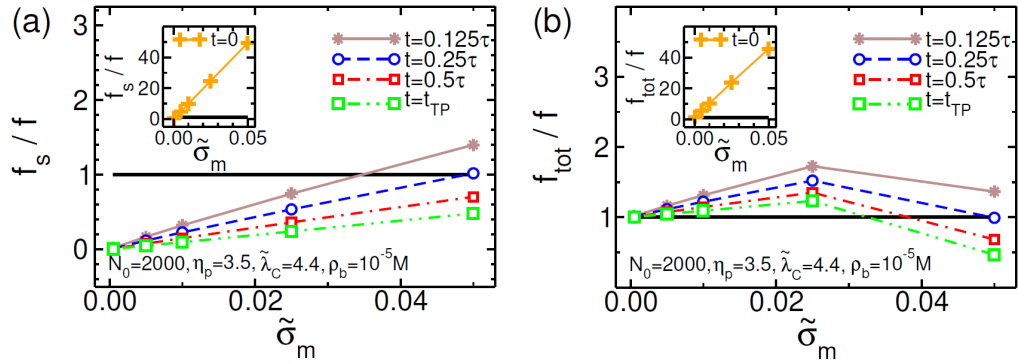


FIG. 4: (a) Normalized electrostatic force due to the charged sphere  $f_s/f$ , as a function of the surface charge density  $\tilde{\sigma}_m$  at different instants of time indicated in the legend in units of the total translocation time  $\tau$ . The external driving force is  $f = 100$ . The other model parameters are reported in the legend. (b) The equivalent of the plot in (a) for the total force  $f_{tot}/f$ .

$\alpha$  as a function of  $N_0$  for various membrane charge and salt strengths. In agreement with the results above, the comparison of Figs. 3 (a)-(c) shows that as the increase of the salt concentration suppresses electrostatic interactions in the system, the trend of the translocation exponent for different values of the surface charge density becomes similar to that of an uncharged system (black open circles). As a result, the non-trivial behavior of the exponent  $\alpha$  appears in the highly dilute salt concentration regime  $\rho_b \lesssim 10^{-4}$  M. Figures 3(a) and (b) indeed show that as the surface charge density increases, the translocation exponent becomes a non-monotonic function of the membrane charge  $\sigma_m$  and the chain length  $N_0$ .

According to Figs. 3(a) and (b), for short polymers with length  $N_0 \lesssim 500$ , the membrane charge strength lowers the scaling exponent, i.e.  $\sigma_m \uparrow \alpha \downarrow$ . For long polymers  $N_0 \gtrsim 500$ , the exponent increases with the membrane charge ( $\sigma_m \uparrow \alpha \uparrow$ ) and exceeds its upper bound  $\alpha = 2$  observed for the uncharged system. We now focus on the non-monotonic polymer length dependence of the exponent  $\alpha$ . One sees that with the increase of the polymer length, the exponent initially rises ( $N_0 \uparrow \alpha \uparrow$ ),

reaches a peak at the characteristic length  $N_0^*$ , and subsequently drops in the long polymer regime ( $N_0 \uparrow \alpha \downarrow$ ). We finally note that the characteristic length for the maximum of the exponent  $\alpha$  is lowered by added salt, i.e.  $\rho_b \uparrow N_0^* \downarrow$ .

The above results provide us with an important set of predictions that can be verified by current translocation experiments. In order to shed light on the physical mechanism behind these electrostatic effects, we show in Figs. 4(a) and (b) the normalized electrostatic force component  $f_s/f$  induced by the electrostatic sphere-membrane attraction and the normalized total force  $f_{tot}/f$ , respectively, as a function of the membrane charge density at different instants of time. The main plot of Fig. 4(a) indicates that during the entire translocation process, the relative weight of the force component associated with the sphere increases with the membrane charge density, i.e.  $\sigma_m \uparrow f_s \uparrow$ . The inset of Fig. 4(a) shows that this effect is particularly pronounced at the beginning of the translocation process (i.e. after the blob nucleation time [25]) where one has  $\tilde{l} \approx 3$  and the sphere has its maximum size. As a result, at the membrane charge density  $\tilde{\sigma}_m = 0.05$ , the electrostatic force acting on the charged sphere is 50

times larger than the external force  $f$ .

These results indicate that the beginning of the translocation process is largely governed by the sphere-membrane interactions. This peculiarity stems from the high monomer number and charge density inside the confined sphere region than on the *cis* and *trans* polymer portions of linear conformation. We have also considered much larger values of  $N_0$  and indeed the early-time sphere-membrane interaction can become huge at dilute salt where screening is weak (data not shown here). During the translocation process, the sphere gradually melts away and its contribution to the translocation dynamics weakens. As a result, Fig. 4(a) shows that the sphere component of the force diminishes with increasing time, i.e.  $t \uparrow f_s \downarrow$ .

Finally, in Fig. 4(b), we show that the net electrostatic force on the polymer varies non-monotonically with the membrane charge strength. Namely, due to the amplification of the sphere contribution, the total force initially rises with the membrane charge ( $\sigma_m \uparrow f_{\text{tot}} \uparrow$ ) and reaches a peak located at  $\tilde{\sigma}_m = \tilde{\sigma}_m^* \approx 0.025$ . Beyond the characteristic membrane charge strength  $\sigma_m^*$ , the electrostatic attraction on the translocated polymer portion in the *cis* direction takes over the sphere attraction in the *trans* direction. As a result, the net electrostatic force decreases with the membrane charge ( $\sigma_m \uparrow f_{\text{tot}} \downarrow$ ). Fig. 4(b) indeed shows that the decreasing branch of the total force curve is absent at the initial instant of time  $\tilde{t} = 0$  (inset), and the drop of the force curve becomes more pronounced with time as the *trans* portion of the polymer gets longer (main plot). The corresponding competition between the force components on the sphere and trans portions of the polymer may be used to control the polymer translocation time by tuning the membrane charge strength via the acidity of the electrolyte solution.

#### IV. SUMMARY AND DISCUSSIONS

An electrostatically augmented IFTP theory has been introduced to investigate the end-pulled charged polymer

translocation through a nanopore embedded in an oppositely charged membrane. It was found that the electrostatic effects on the translocation dynamics is governed by the competition between the membrane-polymer coil coupling force oriented in the trans direction, and the electrostatic force on the translocated portion of the polymer oriented in the opposite *cis* direction. According to our results, the beginning of the translocation process that plays a decisive role in the entire translocation event is governed by the electrostatic membrane-polymer coil attraction. The increase of the membrane charge strength amplifies this attraction and reduces the polymer translocation time, while added salt screens the attractive interaction and rises the translocation time.

We also found that the same electrostatic interactions result in the non-monotonic behavior of the translocation time exponent  $\alpha$ . Namely, for short polymers  $N_0 \lesssim 500$ , the increment of the membrane charge drops the exponent  $\alpha$  towards its lower bound  $\alpha = 1$ . In the long polymer regime  $N_0 \gtrsim 500$ , the exponent rises with the membrane charge and exceeds its upper limit  $\alpha = 2$  previously observed for the charge-free system [33]. Finally, we showed due to the electrostatic polymer-membrane coupling, the translocation exponent rises with the chain length for short chains but drops with the monomer number in the long polymer regime. We emphasize these predictions can be easily tested by current translocation experiments and also contribute to the improvement of our control over the polymer translocation dynamics in next generation biosensing techniques.

#### Acknowledgments

T.A-N. has been supported in part by the Academy of Finland through its PolyDyna (no. 307806) and QFT Center of Excellence Program grants (no. 312298). We acknowledge the computational resources provided by the Aalto Science-IT project and the CSC IT Center for Science, Finland.

- 
- [1] M. Muthukumar, *Polymer Translocation* (Taylor and Francis, 2011).
  - [2] A. Milchev, J. Phys.: Cond. Mat. **23**, 103101 (2011).
  - [3] V. V. Palyulin, T. Ala-Nissila and R. Metzler, Soft Matter **10**, 9016 (2014).
  - [4] J. Sarabadani and T. Ala-Nissila, J. Phys.: Condens. Matter **30** 274002 (2018).
  - [5] S. Buyukdagli, J. Sarabadani and T. Ala-Nissila, Polymers **11**, 118 (2019).
  - [6] S. M. Bezrukov, T. Vodyanoy A. V. Parsegian, Polymers **370**, 279 (1994).
  - [7] J. J. Kasianowicz, E. Brandin, D. Branton and D. W. Deamer, Proc. Natl. Acad. Sci. **93**. 13770 (1996).
  - [8] A. Meller, L. Nivon and D. Branton, Phys. Rev. Lett. **86**, 3435 (2001).
  - [9] K. Luo, T. Ala-Nissila, S.-C. Ying and A. Bhattacharya, Phys. Rev. Lett. **100**, 058101 (2008).
  - [10] G. Sigalov, J. Comer, G. Timp and A. Aksimentiev, Nano Lett. **8**, 56 (2008).
  - [11] J. A. Cohen, A. Chaudhuri R. Golestanian, Phys. Rev. X **2**, 021002 (2012).
  - [12] A. Meller, J. Phys.: Cond. Mat. **15**, R581 (2003).
  - [13] A. F. Sauer-Budge, J. A. Nyamwanda, D. K. Lubensky and D. Branton, Phys. Rev. Lett. **90**, 238101 (2003).
  - [14] D. Branton *et al.*, Nature Biotech. **26**, 1146 (2008).
  - [15] A. J. Storm *et al.*, Nano Lett. **5**, 1193 (2005).
  - [16] J. Mathe, H. Visram, V. Viasnoff, Y. Rabin and A. Meller, Biophys. J. **87**, 3205 (2004).

- [17] S. Carson, J. Wilson, A. Aksimentiev and M. Wanunu, *Biophys. J.* **107**, 2381 (2014).
- [18] U. F. *et. al*, *Nature Physics*, **2**, 473 (2006).
- [19] W. Sung W. and P. J. Park, *Phys. Rev. Lett.* **77**, 783 (1996).
- [20] M. Muthukumar, *J. Chem. Phys.* **111**, 10371 (1999).
- [21] J. Chuang, Y. Kantor and M. Kardar, *Phys. Rev. E* **65**, 011802 (2001).
- [22] R. Metzler and J. Klafter, *Biophys. J.* **85**, 2776 (2003).
- [23] A. Y. Grosberg, S. Nechaev, M. Tamm and O. Vasilyev, *Phys. Rev. Lett.* **96**, 228105 (2006).
- [24] T. Sakaue, *Phys. Rev. E* **76**, 021803 (2007).
- [25] P. Rowghanian and A. Y. Grosberg, *J. Phys. Chem. B* **115**, 14127 (2011).
- [26] J. L. A. Dubbeldam, V. G. Rostiashvili, A. Milchev and T. A. Vilgis, *Phys. Rev. E* **85**, 041801 (2012).
- [27] T. Ikonen, A. Bhattacharya, T. Ala-Nissila and W. Sung, *Phys. Rev. E* **85**, 051803 (2012).
- [28] T. Ikonen, A. Bhattacharya, T. Ala-Nissila and W. Sung, *J. Chem. Phys.* **137**, 085101 (2012).
- [29] T. Ikonen, A. Bhattacharya, T. Ala-Nissila and W. Sung, *Europhys. Lett.* **103**, 38001 (2013).
- [30] J. Sarabadani, T. Ikonen and T. Ala-Nissila, *J. Chem. Phys.* **141**, 214907 (2014).
- [31] J. Sarabadani, T. Ikonen and T. Ala-Nissila, *J. Chem. Phys.* **143**, 074905 (2015).
- [32] J. Sarabadani, T. Ikonen, H. Mökkönen, T. Ala-Nissila, S. Carson and M. Wanunu, *Sci. Rep.* **7**, 7423 (2017).
- [33] J. Sarabadani, B. Ghosh, S. Chaudhury and T. Ala-Nissila, *Europhys. Letts.* **120**, 38004 (2017).
- [34] T. Sakaue, *Polymers* **8**, 424 (2016).
- [35] T. Menais, S. Mossa and A. Buhot, *Sci. Rep.* **6**, 38558 (2016).
- [36] H. W. de Haan and G. W. Slater, *J. Chem. Phys.* **136**, 204902 (2012).
- [37] M. G. Gauthier and G. W. Slater, *Phys. Rev. E* **79**, 021802 (2009).
- [38] I. Huopaniemi, K. Luo, T. Ala-Nissila and S.-C. Ying, *Phys. Rev. E* **75**, 061912 (2007).
- [39] S. Buyukdagli and T. Ala-Nissila, *J. Chem. Phys.* **147**, 114904 (2017).
- [40] S. Buyukdagli, *Soft Matter* **14**, 3541 (2018).
- [41] S. Buyukdagli, *Phys. Rev. E* **97**, 062406 (2018).
- [42] S. Buyukdagli and T. Ala-Nissila, *Europhys. Lett.* **123**, 38003 (2018).
- [43] S. Buyukdagli, J. Sarabadani T. Ala-Nissila, *Polymers* **10**, 1242 (2018).
- [44] P. Margaretti and G. Oshanin, *Polymers* **11(2)**, 251 (2019).
- [45] S. Qiu, Y. Wang, B. Cao, Z. Guo, Y. Chen, G. Yang, *Soft Matter* **11**, 4099 (2015).
- [46] D. P. Hoogerheide, B. Lu, J. A. Golovchenko, *ACS Nano* **8**, 738 (2014).